Chapter 3 : Stainless Steel

As mentioned in Chapter 1, nickel superalloys are generally the material of choice for molten salt reactors. This is predominantly due to their use in the ARE and MSRE during the 1950's and 60's. Work at the time dismissed stainless steel, but further information is scarce [1].

In this chapter stainless steel 316L will be examined, due to its widespread availability and low cost. The composition was determined via ICP-OES and combustion methods and is given in Table 3.1.

Table 3.1: Elemental composition (wt. %) of stainless steel 316L determined by ICP-OES and combustion methods by Element Materials Technology. The values for the elemental composition of iron were calculated by difference.

	Fe	Cr	Ni	Mn	Mo	Si	C	P	S
Stainless steel 316L	69.59	16.36	10.14	1.35	2.13	0.37	0.02	0.033	<0.003

It is envisaged that this chapter will allow some insight into the utilisation of the most commonly used stainless steel grade as a possible material of construction for molten salt reactors.

Figure 3.1 gives a SEM image of the stainless steel before immersion into the molten salt, the surface is clean with some scratches present due to polishing.
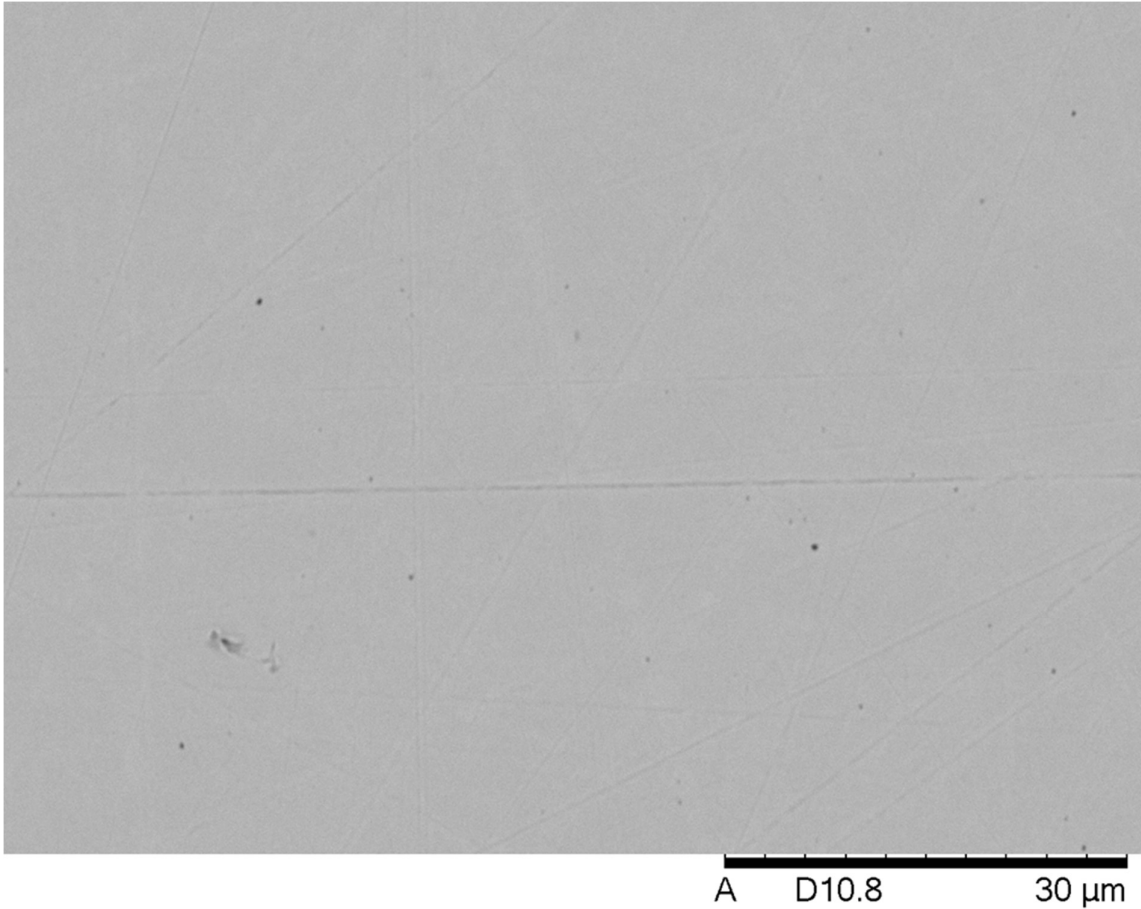
Figure 3.1: SEM image of stainless steel 316L before immersion in the molten salt.

3.1: Baseline Tests

The baseline tests were run for one day in the environment outlined in Section 2.3.1.1, and then samples were taken for analysis. This aimed to ensure that stainless steel 316L, which was initially deemed unsuitable as a material of construction, could withstand the molten salt environment. Images of the resultant samples are given in Figure 3.2.

	Stainless Steel 316L		
1 day			

Figure 3.2: One day baseline test.

The visual results show the formation of a brown/grey layer on the surface, which appears to have served as a protective layer to prevent further corrosion. This directly contradicts work published by

Shankar and Mudali [2] where stainless steel 316L was examined for 25 hours in a LiCl-KCl mix, and chloride attacked the protective layer leading to more aggressive corrosion [2]. The removal of the protective layer due to chloride is also observed by other authors [3-5].

3.1.1: XRD

The XRD pattern for the one day test, along with a sample of stainless steel 316L, are shown in Figure 3.3. Peaks at approximately 44 and 51° 2θ are assigned to stainless steel 316L. The peak at ~18° 2θ is due to the presence of lithium in the form of a spinel on the surface.

It appears that the steel sample in the one day test utilised lithium to form a protective layer over the surface of the sample. It is difficult to ascribe the peak to a particular spinel, as lithium chromium oxide, lithium manganese oxide and lithium chromium manganese oxide all give similar diffraction patterns, this is shown in Figure 3.4, and is further exaggerated by the presence of stainless steel giving a somewhat noisy pattern, which subsequently causes some broad peaks.
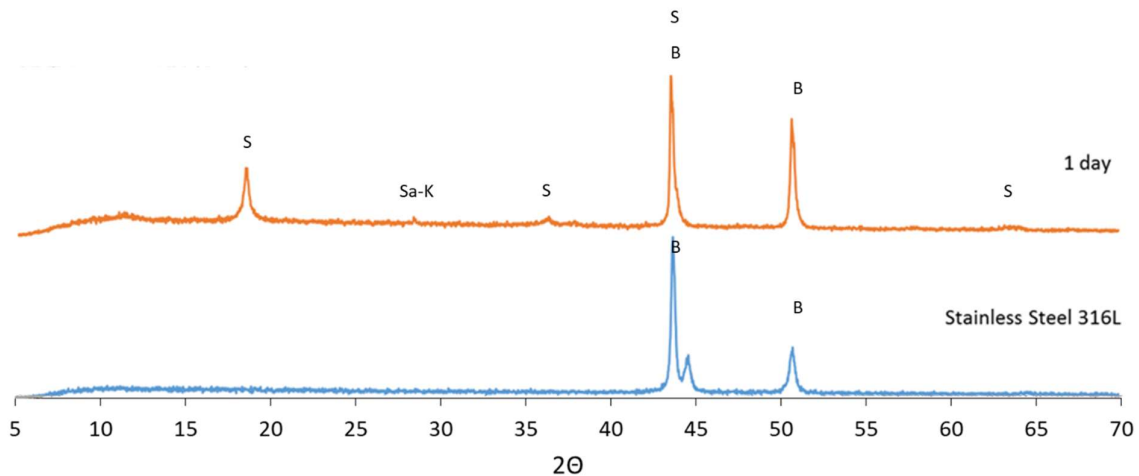

Figure 3.3: XRD patterns for the baseline stainless steel 316L tests. Here S corresponds to a spinel (shown in Figure 3.4), B is the bulk and Sa-K is the potassium salt.
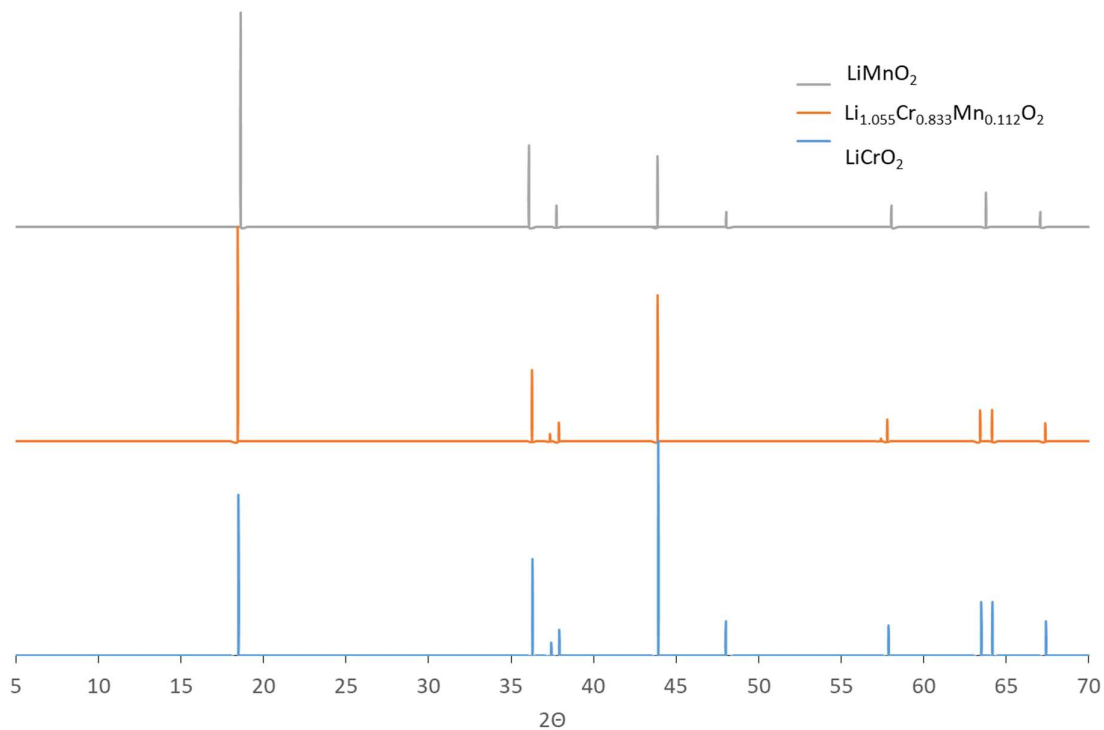
Figure 3.4: Diffraction patterns for possible spinels observed in this work.

3.1.2: SEM/EDX and Cross Sectional Analysis

Three different regions are observed in the one day baseline results, and these are denoted (a), (b) and (c). Figure 3.5 shows a surface SEM image for the one day test; contrast can be seen between the three regions, which are present in conjunction with one another. The EDX analysis for region (a) indicates that it is iron rich and is likely the stainless steel bulk. Grain boundary attack was stated by Richardson et al. [1] to be the predominant form of corrosive attack in Inconels by fluorides [1] and this type of mechanism is visible in area (a). Region (b), also showcased in Figure 3.5, shows a chromium/oxygen corrosion layer. The preferential leaching of chromium has been widely reported in this field, with Richardson et al. [1] reporting that voids are formed due to the depletion of chromium, this has also been observed by Shankar and Mudali, and by Olson et al. [1, 2, 6]. The experiment was run in atmospheric conditions and it was therefore possible for oxygen to aid in the formation of the corrosion layer, whereas work by other authors has generally been conducted in a controlled environment and the effect of oxygen has been minimal [2, 6, 7]. The corrosion layer does not cover the full sample, but where the corrosion product is present the bulk Figure 3.5 is not observable. This suggests that the corrosion product is relatively thick and while it does not cover the full sample, it is envisaged that as the immersion time increases so will the surface coverage. The

formation of only one oxide contradicts the work done by Subari et al. [8], where numerous oxides were formed after an immersion time of 24 hours [8].

Figure 3.5 shows a textured surface denoted as region (c), the EDX analysis shows that iron is the main element present, and it is believed that the stainless steel bulk (a) was attacked. This is further proven by the difference in the microstructure of area (a) and (c): (a) appears smooth, whereas (c) is more textured. This textured surface suggests that the bulk has been attacked, and it is believed that the alloying elements have been sacrificially removed from the stainless steel bulk (a) to form (c) before the corrosion layer, (b).

Sodium and potassium are shown in the EDX data to represent alkali metals from the eutectic salt; lithium cannot be observed in the EDX data as it has a low atomic number and cannot be detected, but when analysed together with the XRD data it is likely that a lithium chromium oxide layer has formed.
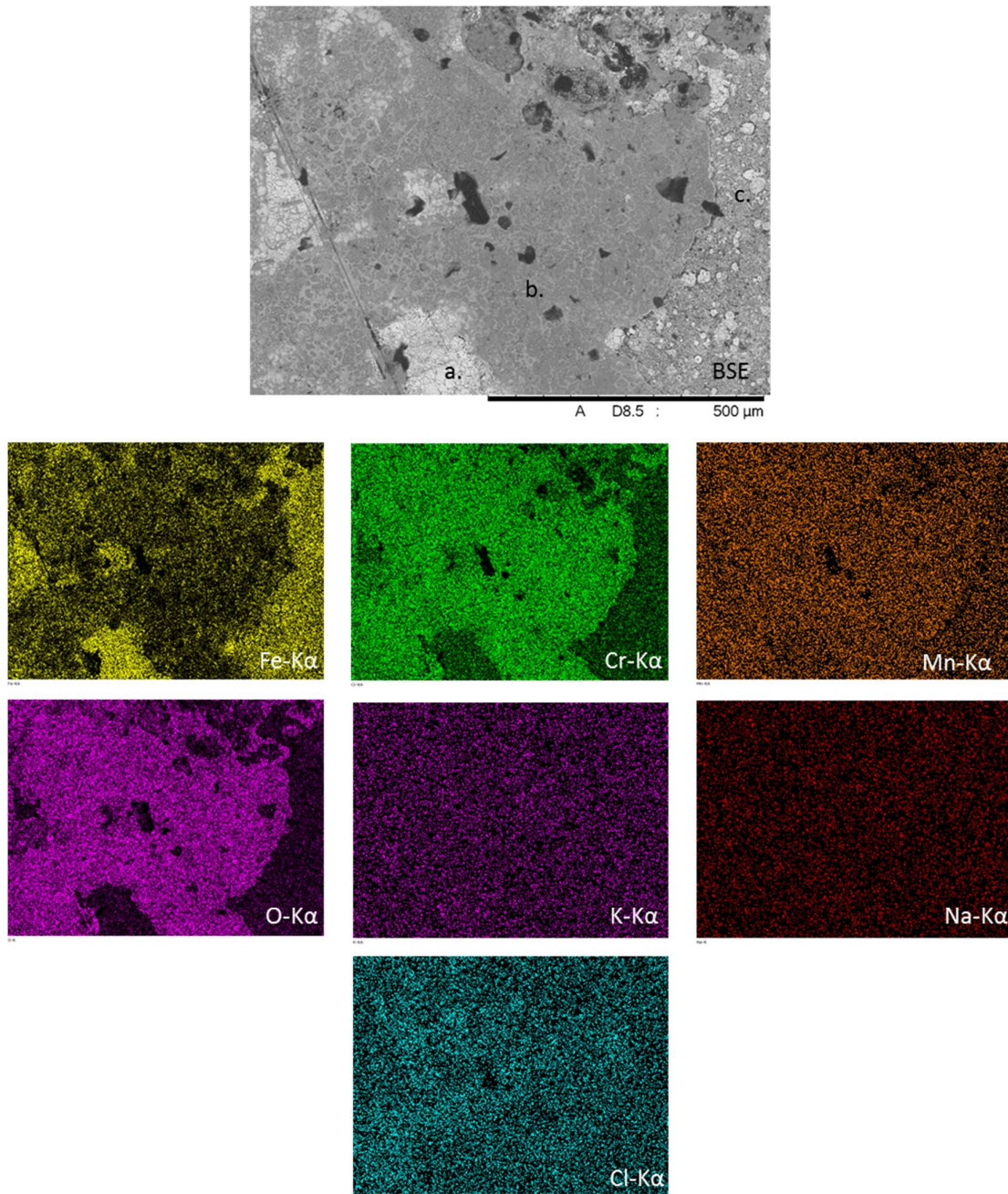
Figure 3.5: BSE image and corresponding EDX elemental maps for stainless steel 316L coupon immersed in an alkali eutectic chloride salt for one day. Regions (a), (b) and (c) are discussed in the text.

On a first viewing, Figure 3.5 suggests that manganese is present within the corrosion layer, as contrast can clearly be seen in the EDX data for manganese. However, the preferential leaching of manganese has not been observed in the literature and therefore further investigation was required. Figure 3.6 shows the EDX spectrum between 5-6.6 keV. The K_β peak for chromium is observed at 5.95 keV, whereas the K_α peak for manganese is observed at 5.9 keV, and as broad peaks are obtained for this sample, it is easy for the two elements to be present within the EDX data, but further investigation

does suggest that only chromium is present [9]. It is therefore highly likely that manganese present in EDX data has been incorrectly quantified by the software.
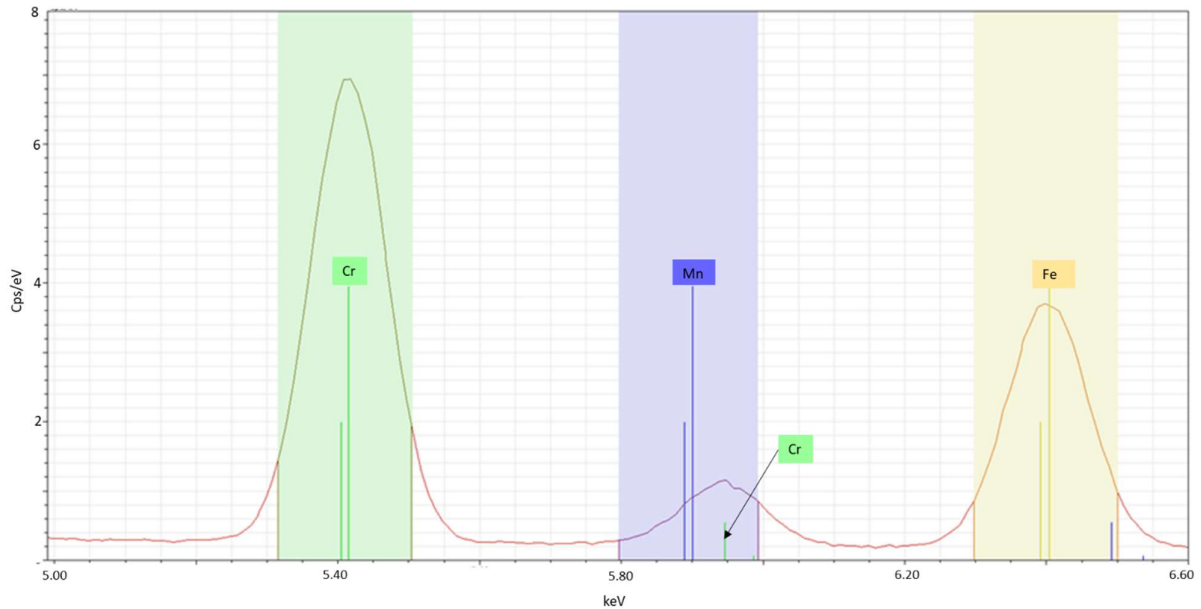

Figure 3.6: EDX spectral peak positions and integration regions for chromium, manganese and iron between 5-6.6 keV, along with an example spectrum obtained for the sample.

EDX can also be used to give an estimation of the composition of the layer, this is given in Table 3.2. This reiterates the results that have already been observed, with an increase in the relative composition of the chromium and oxygen in area (b), when compared to area (a) and (c). The point analysis gave no indication that manganese was present within area (b).

Table 3.2: Estimation (at. %) of the composition for areas a, b and c shown in Figure 3.5. This was obtained from EDX data.

	a	b	c
Iron	48.9		35.3
Carbon	15.3	15.9	26.9
Nickel	14.3	5.4	13.4
Chromium	12.5	40.8	12.6
Oxygen	9.11	38.0	11.8

The cross sectional image, Figure 3.7, does not give much insight into the corrosion layer. This is seen throughout this work, and is to be expected as the layer appears sporadically on the surface. Although the layer appears thick in Figure 3.5, it is relatively thin when compared with the bulk and is difficult to observe. Images were taken at a higher magnification, but have a low resolution and any corrosion

product is difficult to distinguish. It is also possible that due to the sporadic nature of the layer there is no corrosion product present within the analysed area.
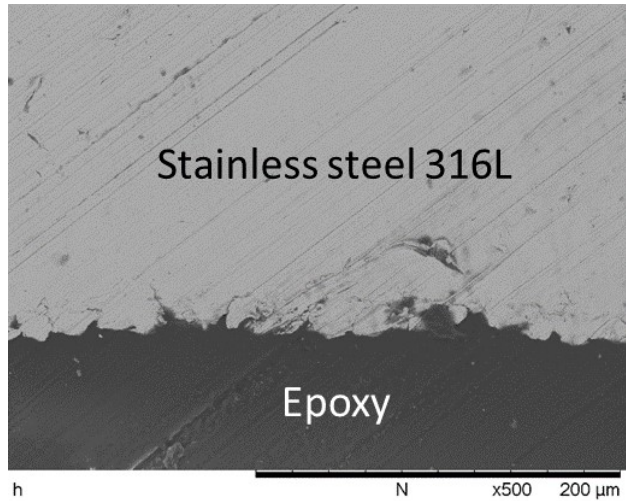

Figure 3.7: Cross-sectional BSE image for a stainless steel 316L coupon immersed in a molten alkali chloride eutectic for one day.

The SEM/EDX results combined with the XRD patterns obtained for the one day test show that it is possible for stainless steel 316L to withstand the extreme environment in a molten chloride bath. The data suggest that a lithium spinel has been formed, with the predominant metal being chromium. It is thought that $LiCrO_2$ has been formed as a protective layer. Previous work has stated that chromium is preferentially leached, but the utilisation of lithium to aid in the formation of a protective layer has not been seen.

3.2: Stainless Steel 316L Tests

Once it was established that stainless steel 316L could endure the extreme environment created in the molten chloride salt bath, further tests could be conducted. As stipulated in the literature, between 500 and 1000 hours (approximately three and six weeks) the corrosion rate levels out [1, 10], therefore tests were run for one, three, four and six weeks in the same conditions as the baseline test. One and four week tests were added to give further information between the two time frames.

The results of these experiments can be seen in Figure 3.8.

1 week			
3 weeks			
3 weeks (trial)			
4 weeks			
6 weeks			

Figure 3.8: Stainless steel results obtained (from top to bottom: one, three, three week repeat (denoted as trial in the image), four and six weeks).

The visual results show an anomalous result at three weeks with the formation of a black highly textured surface, despite the experiments running in the same environment. This type of product has previously been observed by Sellers et al. [3], where a FLiNaK salt was used at 850°C and due to a failure in one of the crucibles the molten salt reacted with the silicon carbide insulation within the furnace, which resulted in the formation of K_2NaCrF_6 and hematite [3]. The three week samples also show a loss of toughness and can easily be broken. At first this was believed to be an anomalous result, but throughout this work unusual results are observed several times at an exposure duration of three weeks, and this will be discussed further in Section 6.5. The three week test was repeated and the anomalous result was not observed. The other results are visually consistent and show a dull grey

corrosion product formed on the sample. Kruizenga states that a stable corrosion layer cannot be formed in a chloride molten salt when impurities are present [11], this implies that the initial three week tests are actually more representative of the expected result. Figure 3.8 appears to dispute this (if the three week test is omitted) with the formation of a consistent corrosion layer over all samples. The main difference in Kruizenga's work compared to the work in this report is the presence of lithium within the molten salt.

Figure 3.9 shows that the mass loss is close to linear for the samples. It should be noted that the mass change of the specimen is due to loss of initial material and formation of corrosion product. Mass change measurements were not taken for the original three week test.
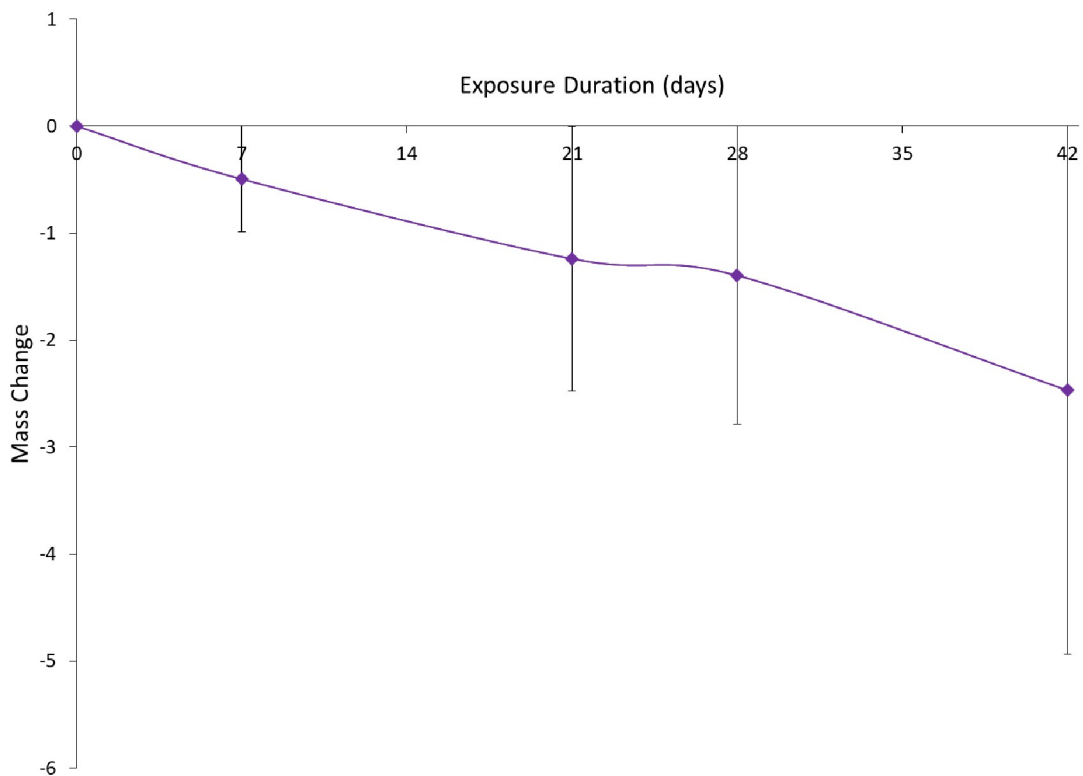

Figure 3.9: Mass loss of the stainless steel samples during corrosion, as a percentage of initial coupon mass; the original three week test is not shown.

3.2.1: XRD

The diffraction patterns for the studied samples can be seen in Figure 3.10; the peaks at approximately 44 and 51° 2θ are assigned to stainless steel 316L. These peaks are present in all the samples but have a significantly lower intensity as immersion time increases, which is attributed to the thicker corrosion layer. Four of the five patterns show the presence of a lithium-containing product at approximately

18°, this strongly suggests that a lithium chromium oxide is present, as seen in the baseline test, but further analysis via EDX is required to confirm this.

The lithium-containing spinel peak at approximately 18° 2θ is not present in the three week test. In addition to the two peaks assigned to stainless steel 316L there are numerous oxides including those of iron (Fe_3O_4, FeO), chromium (Cr_2O_3), and iron and chromium ($Cr_{0.75}Fe_{1.25}O_3$). It is also possible that $KCrO_2$ and $FeCl_2$ are present, but with peak broadening, this is difficult to confirm.

The diffraction pattern also indicates that salt is present in the sample, but due to the highly textured surface and inefficient packing of the corrosion product there is a likelihood that it is trapped within the system. This is also possible within the repeated three week test along with the four and six week test, where it is envisaged that a thicker corrosion product will be formed due to longer immersion time.

It appears that the majority of the tests utilise lithium to form a protective layer over the surface of the sample, whereas the three week sample has not. Similar results were obtained by Sellers et al. [3] who saw the utilisation of sodium and potassium containing compounds within the corrosion products formed in their work; despite lithium being present it was not observed to be incorporated into these corrosion products [3].
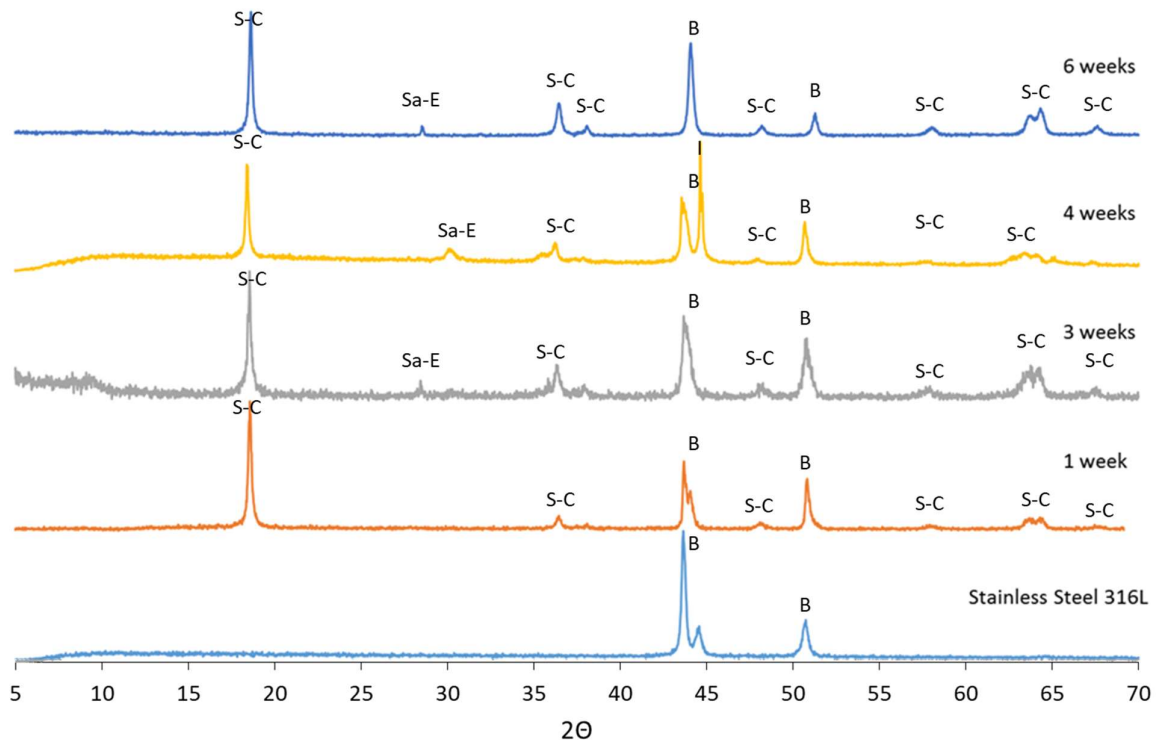

Figure 3.10: XRD patterns for the stainless steel 316L reruns, where S-C corresponds to the spinel $LiCrO_2$, Sa-K is KCl, B is the bulk, Sa-Eu is the eutectic salt, IO is iron (III) oxide and Sa-Na is NaCl.

3.2.2: SEM/EDX
　　3.2.2.1: Surface SEM/EDX

The SEM images obtained in the stainless steel tests show similar results to one another and to the baseline tests, if the three week test is omitted. Therefore the one, three week (repeat), four and six week samples will be reported together, and the three week tests will be reported in Section 3.2.2.3 and 3.2.2.4. Figure 3.11 shows the four BSE images obtained for each of the stainless steel samples held in the molten chloride for a predetermined length of time. Their EDX data is very similar and therefore only the six week test will be shown, Figure 3.12.
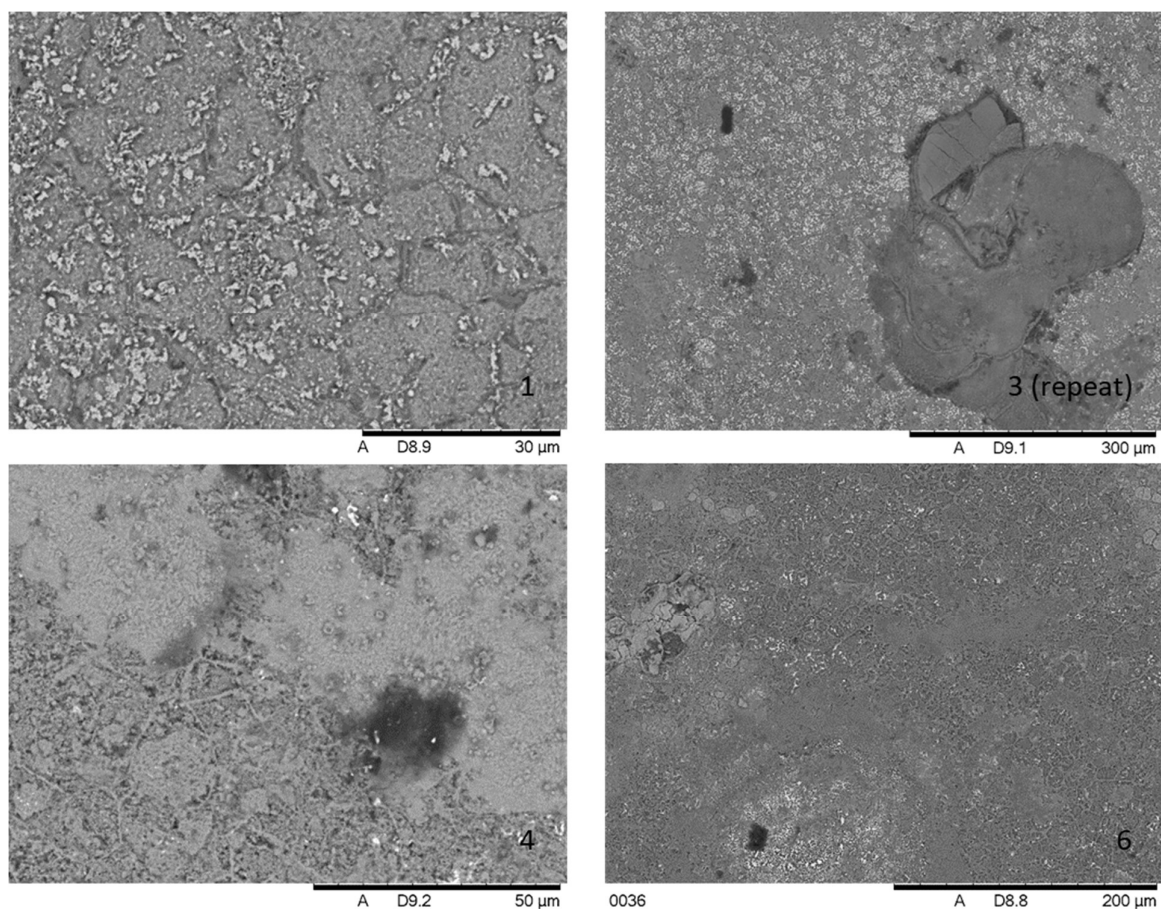
Figure 3.11: BSE images of stainless steel 316L held in a molten alkali chloride salt for a predetermined length of time (stated in the bottom right of each image).

The corrosion layers cover the majority of the sample, and the attacked stainless steel surface (c) that was observed in the one day baseline tests is generally not present. Figure 3.12, which shows the six week tests, suggests that chromium and oxygen are present along with iron from the stainless steel, and it is therefore likely that this phase is $LiCrO_2$ denoted as (b) in the baseline tests. The selective leaching of chromium has previously been seen by Shankar and Mudali [2] as well as Reiser et al. [12].

The presence of chromium, not only in the corrosion layer but also along grain boundaries, can be seen in the one week BSE image in Figure 3.11 and is a common phenomenon known as intergranular corrosion [13].

A repeat of the three week test was deemed necessary after the irregular results obtained in the original three week tests. The repeated test resulted in a further area (d) that required further EDX analysis, this is shown in Figure 3.13, and a similar area is observed in the six week tests, Figure 3.12.

The EDX data appear to show that an iron chloride or oxide has formed on both the three week repeat and the six week samples. The XRD patterns for the three (repeat) and six week tests do not show the presence of an iron compound, which has been identified in the EDX data. It is possible that these products are present within the diffraction pattern, but due to disordered phases in the data they are difficult to identify. Furthermore, Table 3.3 also shows an estimate of the elemental composition of (d) obtained via point analysis for both the three week repeat and six week tests and appears to show the formation of an iron oxide. This was difficult to conclude from the EDX due to the lack of contrast within the oxygen data. It is possible that chloride is also present within the sample, but as a trapped inclusion within the disordered matrix.
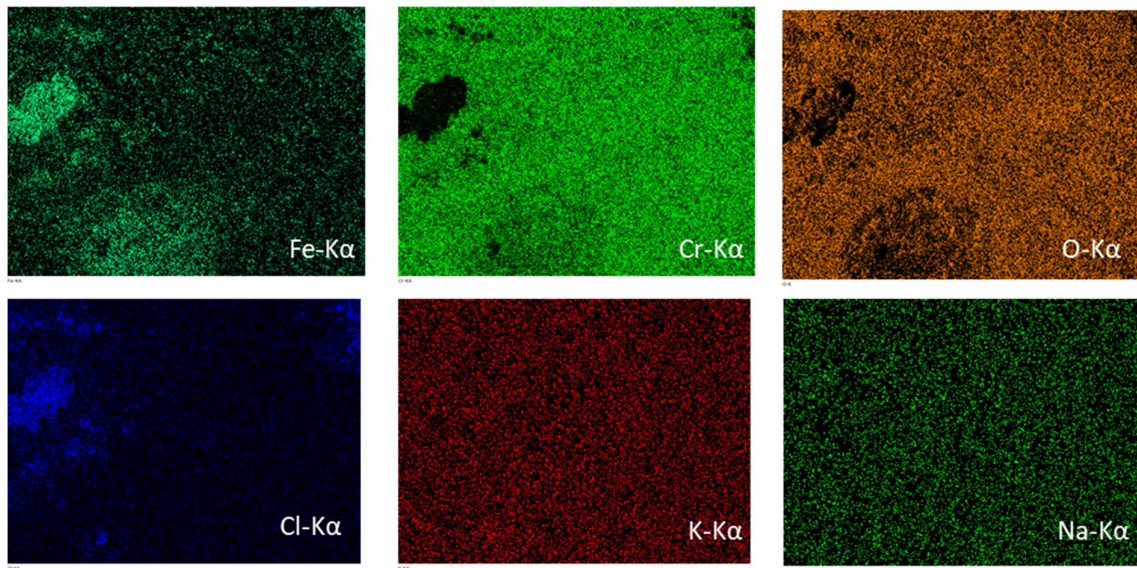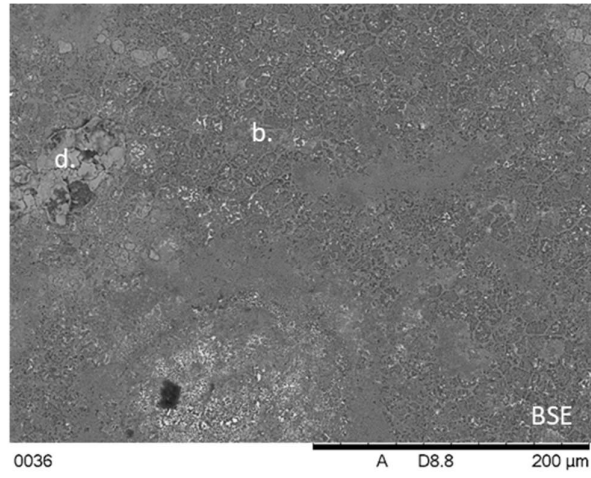
Figure 3.12: BSE image and corresponding EDX elemental maps for the surface of stainless steel 316L coupon immersed in a molten alkali chloride eutectic for six weeks. Region (d) is discussed in the text.
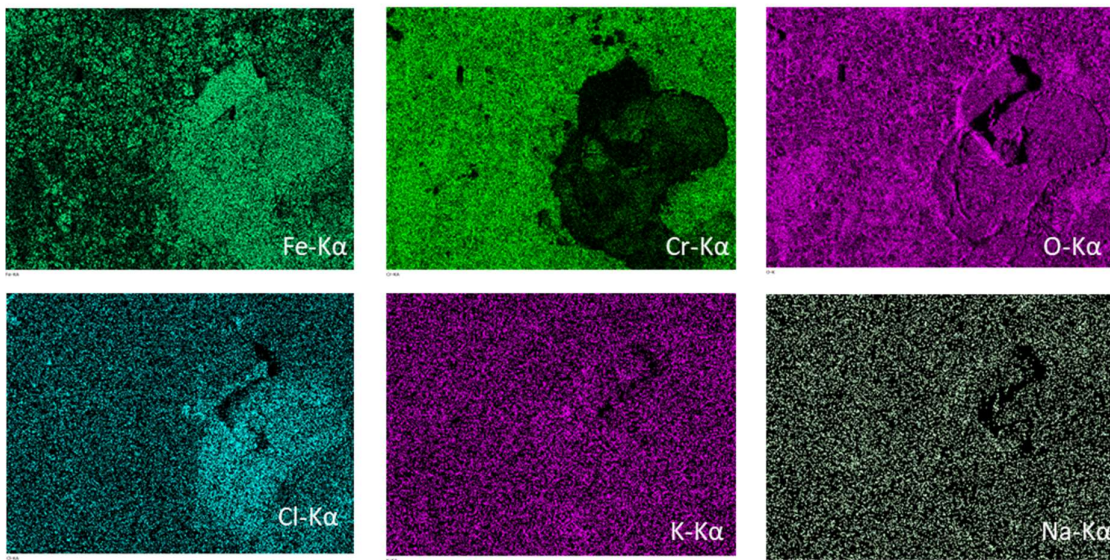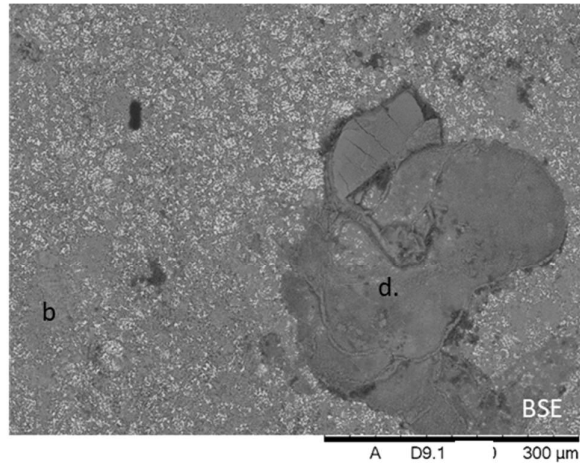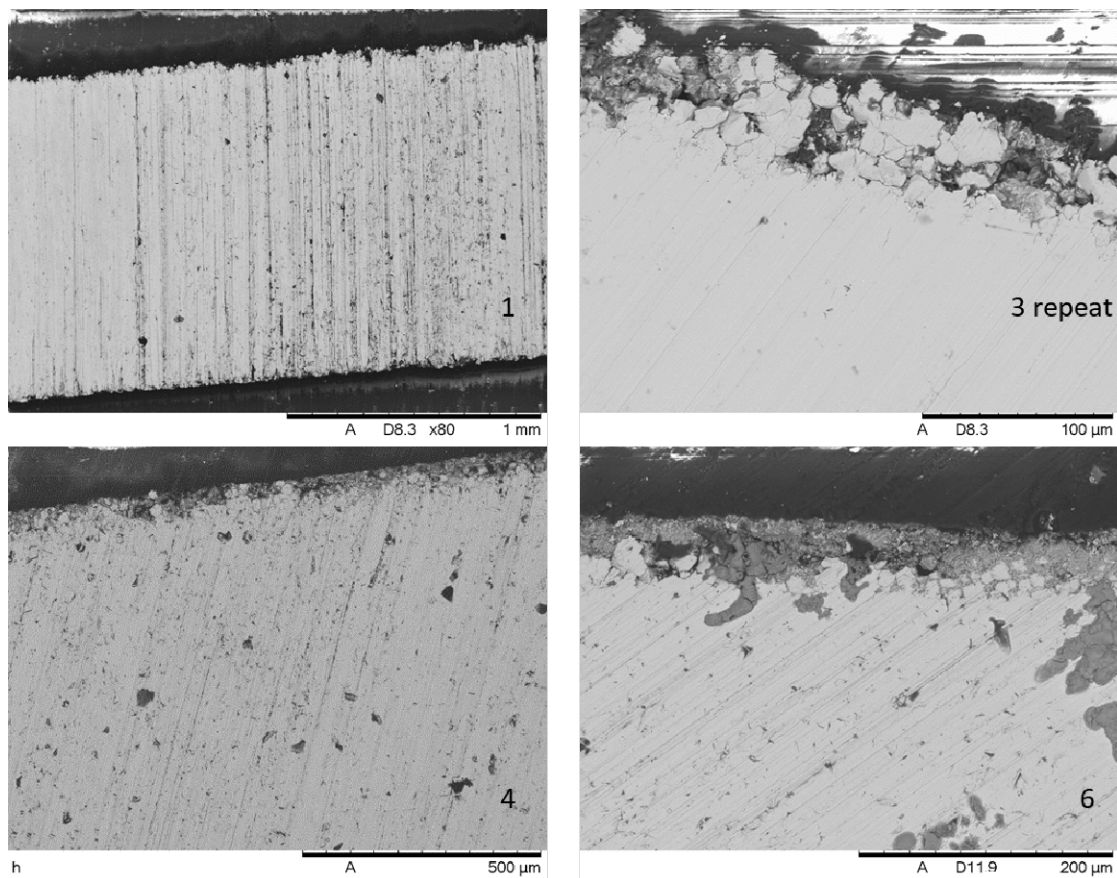
Figure 3.13: BSE image and corresponding EDX elemental maps for the surface of stainless steel 316L coupon immersed in a molten alkali chloride eutectic for three weeks. Region (d) is discussed in the text.

Table 3.3: Estimation of the elemental composition (at. %) of the area marked as (d) in Figure 3.12 and Figure 3.13.

	Three week (repeat) test	Six week test
Oxygen	37.0	35.7
Iron	25.5	23.6
Carbon	13.9	11.4
Nickel	12.4	14.4
Chromium	10.0	2.1
Chlorine	1.3	10.3

3.2.2.2: Cross Sectional Analysis

The cross section SEM can be seen for the one week, repeated three week, four and six week samples in Figure 3.14, and as time progresses it becomes clear that the depth of attack has increased, with attack and subsequent formation of lithium chromium oxide on the surface of the sample. The six week results show further penetration and the EDX data are shown in Figure 3.15. The corrosion layer, (b) a chromium-oxygen layer, is similar to the corrosion layer which appears in the four week test, but the six week test also has areas of iron oxide (d) diffusing further into the bulk. Although there was some ambiguity towards area (d) during surface analysis, the cross sectional EDX clearly shows iron oxide.

Figure 3.14:Cross-section BSE images of stainless steel 316L held in a molten alkali chloride salt for a predetermined length of time (stated in the bottom right of each image).
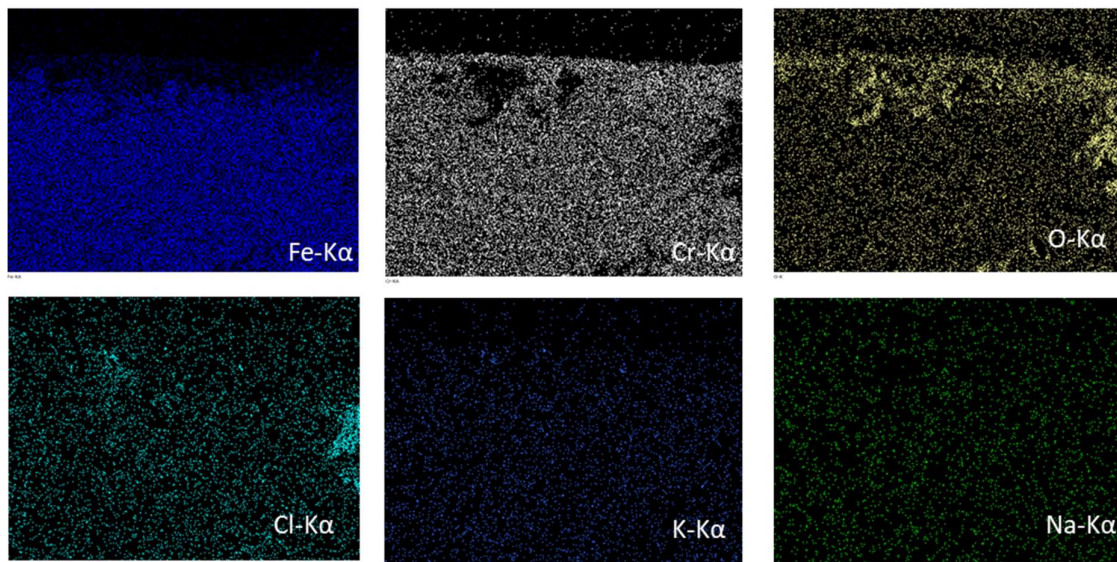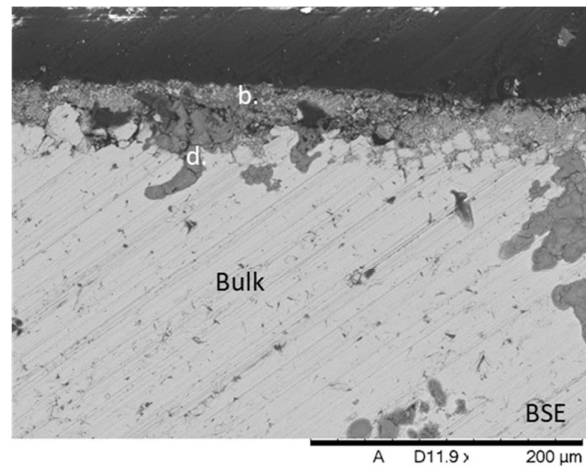
Figure 3.15: cross-sectional BSE image and corresponding EDX elemental maps of the stainless steel 316L coupon immersed in a molten alkali chloride salt for six weeks. Regions (b) and (d) are discussed in the text.

3.2.2.3: Three Week Surface SEM/EDX

Analysis of the three week samples has proven extremely difficult due to the wide breadth of corrosion products that are present. Currently five different corrosion products (e-i) have been identified in the surface SEM images and are shown in Figure 3.16.

Area (e) in Figure 3.17 shows the formation of a 'blocky' crystal corrosion product, and an additional image, Figure 3.16, suggests that the predominant elements present within region (e) are chromium, oxygen and possibly iron. Further point analysis on this area suggests that chromium oxide has formed on the surface. This coincides with previous work, whereby Cr_2O_3 forms a passivating layer over the stainless steel surface [14]. It should be noted that point analysis is an estimate.

Table 3.4: Estimation of the elemental composition (at. %) of the area marked as (e) in Figure 3.16 and Figure 3.17

	Figure 3.16	Figure 3.17
Chromium	36.3	41.9
Iron	18.5	16.8
Carbon	9.4	9.3
Chlorine	1.1	1.0
Oxygen	34.5	30.9

Area (f) is a flat corrosion product, and this is shown in Figure 3.16 and Figure 3.18. The EDX data in Figure 3.18 show little contrast between areas (f) and (g), but the images do suggest that iron, chromium, oxygen and chlorine are involved in the formation of corrosion product (f). Figure 3.16 and Figure 3.19 suggest that chromium is not present in the corrosion layer, only iron and oxygen. Although the elemental composition does appear to vary wildly, the microstructure and morphology of corrosion product (f) is consistent. As previously mentioned the EDX data are difficult to analyse fully in these samples due to the highly textured nature of the sample surfaces. It should also be noted that sodium, incorporated from the molten salt bath, appears to be a lot more prominent in corrosion product (f) compared to the other corrosion products formed.

Point analysis was conducted on area (f) and is shown in Table 3.5. The results were normalised to omit oxygen, although oxygen is present the results show a higher than expected level of oxygen and therefore it has been omitted to allow clearer analysis of the corrosion product.

Table 3.5: Estimation of the elemental composition (at. %) of the area marked as (f) in Figure 3.16 and Figure 3.18.

	As measured			Normalised		
	Figure 3.16	Figure 3.18	Figure 3.19	Figure 3.16	Figure 3.18	Figure 3.19
Oxygen	75.7	71.6	65.4			
Carbon	16.2	16.6	14.5	69.5	58.2	42.9
Iron	3.8	5.4	11.7	16.1	18.9	33.8
Chlorine	1.9	2.9	5.4	8.2	10.2	15.6
Chromium	0.8	0.6	0.9	3.4	2.1	2.6
Silicon	0.6	1	0.8	2.6	3.5	2.3
Molybdenum		2	1.3		7.0	3.8

Point analysis suggests that iron is preferentially leached from the stainless steel, and this coincides with the results obtained via the EDX images. It is clear from these results that chromium is not preferentially leached. This is unusual as it has been widely reported that chromium will leach in these conditions [15-17].

Other experiments within this chapter showed incorporation of lithium into the corrosion product, this is expected as lithium is more reactive than sodium and potassium, and this was observed in work by Cheng et al., who stated that due to the more basic nature of lithium it was incorporated into the corrosion product [18]. Sellers et al., who worked with stainless steel 316L in a molten FLiNaK environment, saw the formation of K_2NaCrF_6. The SEM images obtained by Sellers et al. [3] do not show strong similarities to the images obtained in this section, but some of their concepts have aided in explaining these results. The formation of a potassium containing corrosion product is also observed by Biedenkopf [19] with high alloy steels containing a high chromium content in LiCl-KCl melts at 650°C [19]. Further work showing sodium being utilised in a corrosion product in similar environments has not been found; Subari et al. [8] stated that sodium chloride promotes corrosion, but further information is scarce [8].

Corrosion area (g) is seen throughout the surface SEM results and initially appears to have a similar microstructure to stainless steel 316L, but Figure 3.16-Figure 3.19 all show that in addition to iron, chlorine is also present. Therefore the molten salt has either chemically altered the bulk resulting in an iron chloride layer, or a corrosion product has formed on the surface containing iron and chlorine. It is the only corrosion product that shows consistent results throughout the three week analysis.

The point analysis shown in Table 3.6 gives a further indication of what is present within the system. Iron is consistently seen in each of the images, along with a relatively high composition of chlorine as shown in the point analysis.

Table 3.6: Estimation of the elemental composition (at. %) of the area marked as (g) in Figure 3.16-Figure 3.19.

	Figure 3.16	Figure 3.17	Figure 3.18	Figure 3.19
Oxygen	44.0	40.5	49.8	37.1
Iron	24.0	37.6	16.0	32.5
Chlorine	19.3	9.4	19.9	21.7
Carbon	7.6	9.3	8.8	8.6
Potassium	5.1		1.9	
Chromium		3.2	3.6	

Corrosion product (h) is seen in Figure 3.16 and Figure 3.18. It is more textured compared to corrosion products (f) and (g). Figure 3.18 suggests that iron and oxygen are the main elements, but the nature of these products does make collecting EDX data difficult.

Point analysis of the sample can give further information: if the normalised values are assessed it is difficult to say which anion is present, due to the higher than expected level of oxygen, but it seems likely that iron is the main element.

Table 3.7: Estimation of the elemental composition (at. %) of the area marked as (h) in Figure 3.16 and Figure 3.18.

	As measured		Normalised	
	Figure 3.16	Figure 3.18	Figure 3.16	Figure 3.18
Oxygen	75.8	80.0		
Carbon	17.0	17.5	70.6	87.6
Iron	2.6	1	10.8	5
Chlorine	4	1.2	16.6	6
Chromium	0.5	0.3	2.1	1.5

Corrosion product (i) is present in Figure 3.16 and Figure 3.19, and appears to be an intermixing of corrosion products (e) and (f). Figure 3.19 show the formation of blocky crystals similar to (e) embedded into a flat corrosion product similar to (f). These crystals have previously been observed by Shankar and Mudali [2] and by Sellers et al. [3]. Figure 3.19 shows a high level of contrast between areas (h) and (i), and it appears that chromium, and oxygen are present.

Table 3.8: Point analysis for corrosion product (i) in Figure 3.16 and Figure 3.19.

	As measured		Normalised	
	Figure 3.16	Figure 3.19	Figure 3.16	Figure 3.19
Chromium	1.5	1.9	6.3	7.6
Iron	4.9	6.8	20.6	27.1
Carbon	17.4	16.4	73.1	65.3
Oxygen	75.4	75.0		

The point analysis suggests that iron oxide is the predominant product formed in this particular experiment.

It was also noted that these samples are brittle and have lost toughness. It was therefore deemed necessary to investigate the lattice parameters of the corrosion products along with stainless steel, as a large difference in these could give an indication as to why the sample is under strain. Table 3.9 shows the lattice parameters of the proposed corrosion products that have been formed in the three week tests, and also for comparison the one week test.

Table 3.9: The lattice parameters obtained from PDF4+ for the corrosion products and stainless steel.

	Stainless Steel	Fe_3O_4	Fe_2O_3	$LiCrO_2$	Cr_2O_3
a	3.591	8.375	5.028	2.889	4.958
b	3.591	8.375	5.028	2.889	4.958
c	3.591	8.375	13.730	14.412	13.593
	Cubic	Cubic	Rhombohedral	Rhombohedral	Rhombohedral

The lattice parameters of the corrosion products are all different from each other, suggesting that if brittleness is caused by a physical change it would be observed in both the one week and three week sample. These differences are not enough to cause excessive strain on the sample as seen in the three week samples. It is therefore likely that this is caused by chemical damage to the steel, such as a change to the composition of the steel as the corrosion products have formed.
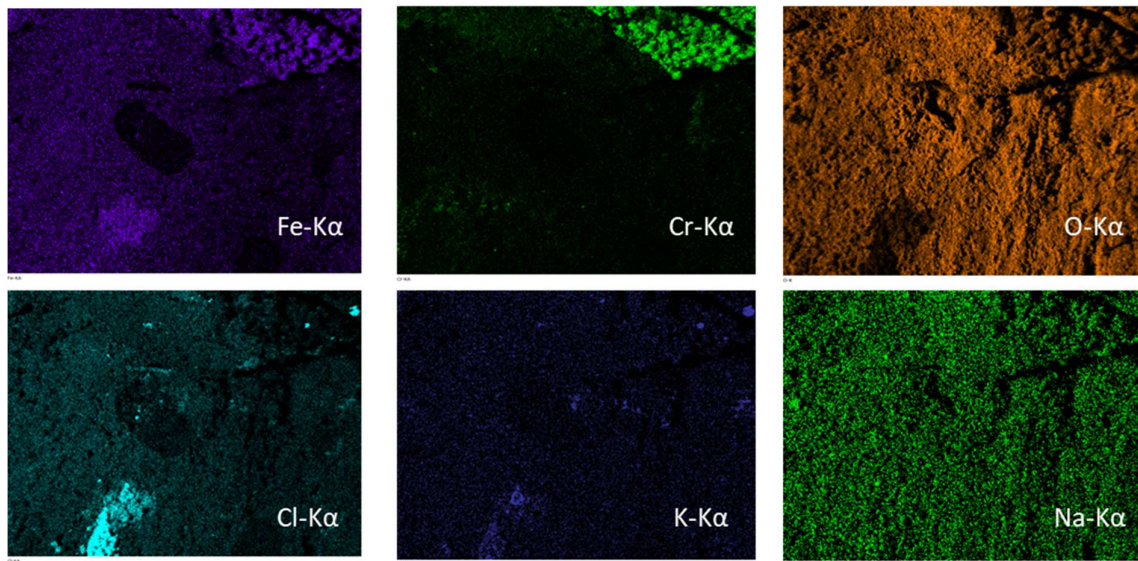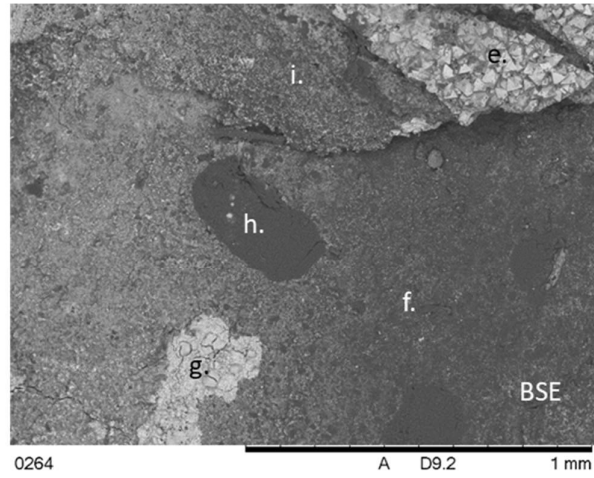
Figure 3.16: BSE image and corresponding EDX elemental maps for the surface of a stainless steel 316L coupon immersed in a molten alkali chloride eutectic for three weeks. Regions (e)-(i) are discussed in the text.
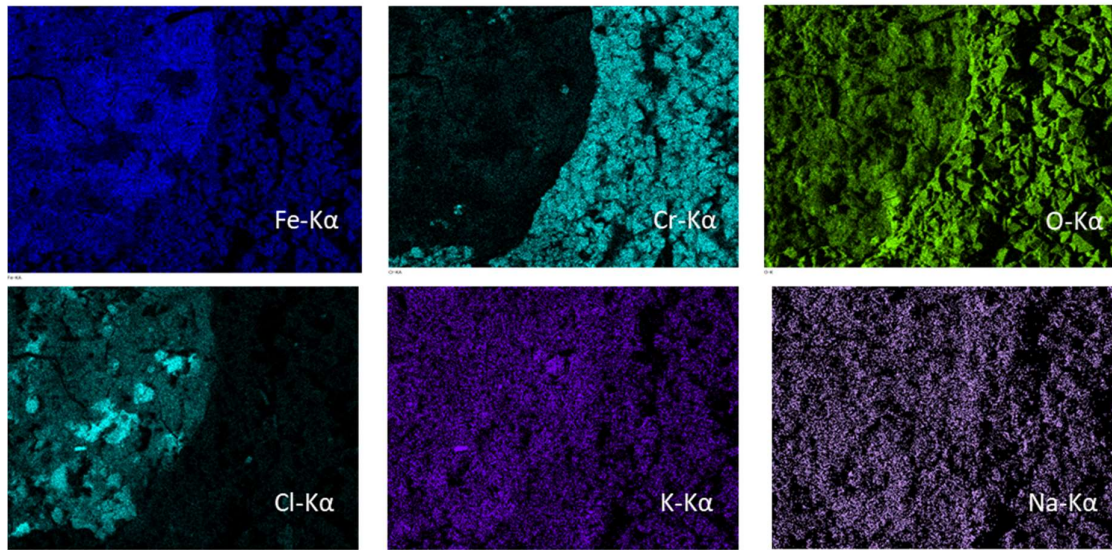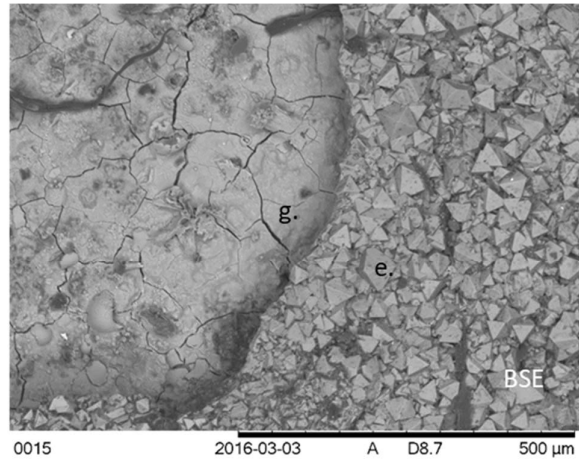
Figure 3.17: BSE image and corresponding EDX elemental maps for the surface of a stainless steel 316L coupon immersed in a molten alkali chloride eutectic for three weeks. Regions (e) and (g) are discussed in the text.
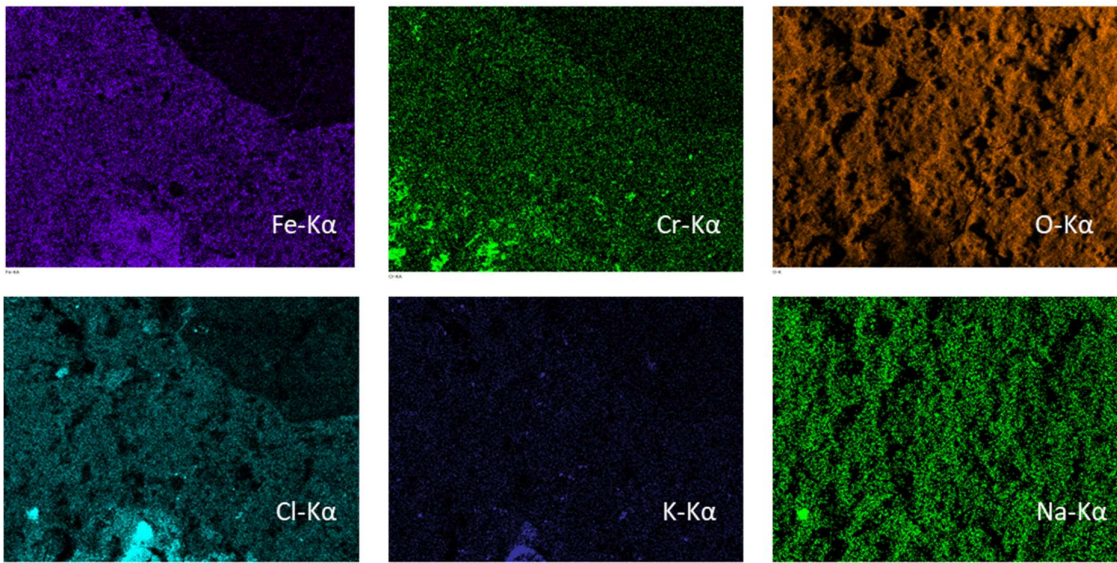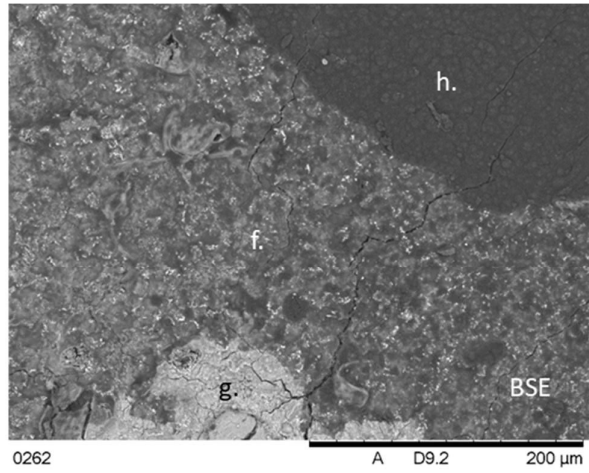
Figure 3.18: BSE image and corresponding EDX elemental maps for the surface of a stainless steel 316L coupon immersed in a molten alkali chloride eutectic for three weeks. Regions (e), (f) and (h) are discussed in the text.
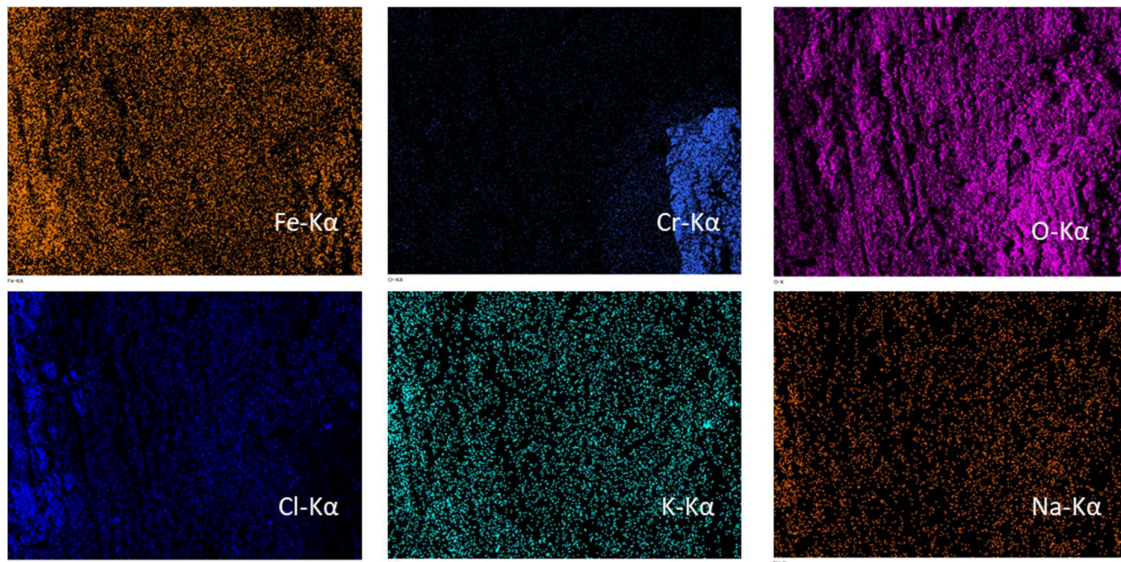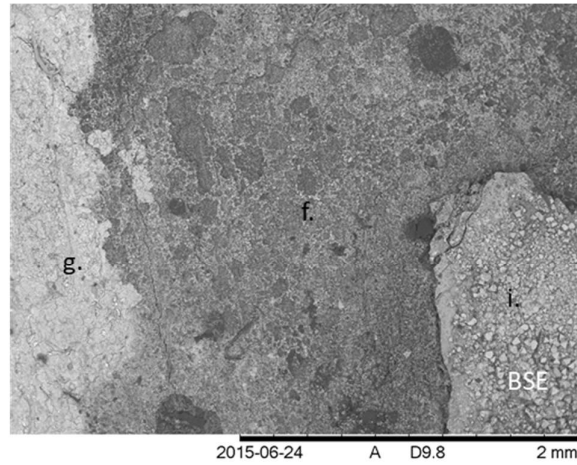
Figure 3.19: BSE image and corresponding EDX elemental maps for the surface of a stainless steel 316L coupon immersed in a molten alkali chloride eutectic for three weeks. Regions (g)-(i) are discussed in the text.

3.2.2.4: Three Week Cross Sectional SEM

The cross sectional SEM/EDX data after three weeks of exposure are shown in Figure 3.20, a chromium layer has formed on top of a thick iron layer. The cross sectional SEM also appears to show sodium chloride trapped within the porous corrosion layer, and explains the higher than normal concentration of sodium in numerous surface SEM images.
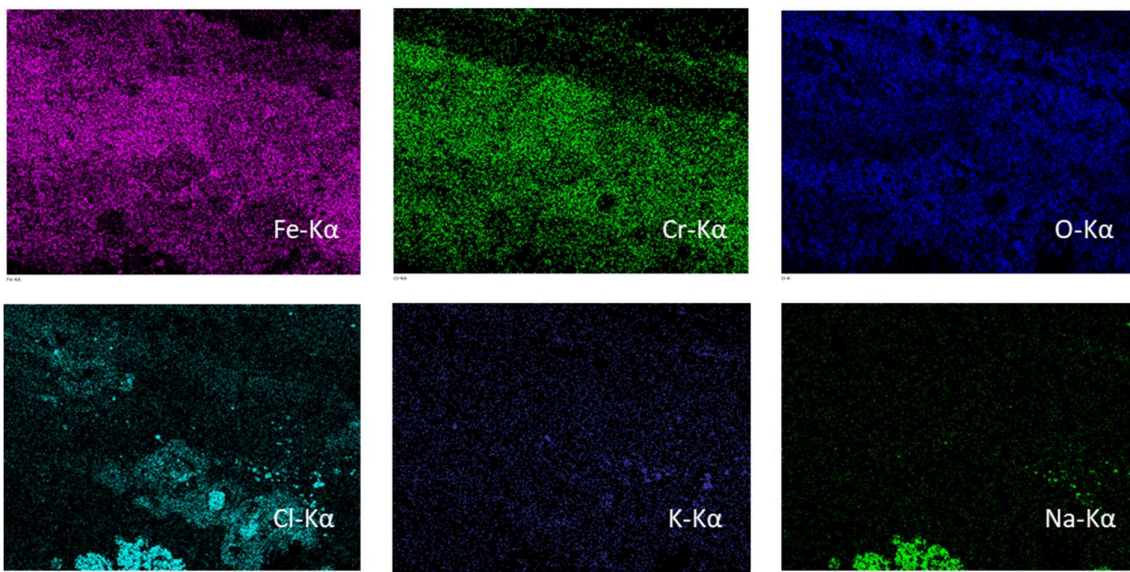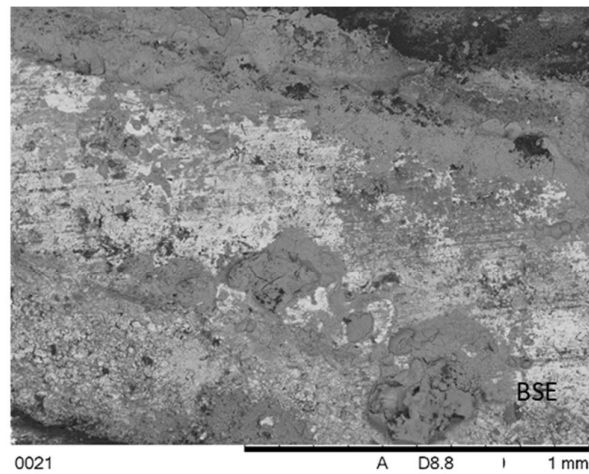
Figure 3.20: Cross-sectional BSE image and corresponding EDX elemental maps for a stainless steel 316L coupon immersed in a molten alkali chloride eutectic for three weeks.

The three week tests have proved difficult to analyse, with numerous different elements present within the same corrosion product. It is clear that numerous different products have been formed and five have been clearly identified. With certainty a blocky corrosion product has been formed, (e), and this appears to be formed via corrosion product (f), which forms corrosion product (i) which subsequently forms (e). Further to this, corrosion product (g) has also been identified as an iron oxide, initially thought to be the stainless steel bulk or iron chloride, but point analysis has indicated that iron oxide appears more likely. Finally, area (h) shows a distinct lack of iron and chromium. A summary of all of the corrosion products is shown in Table 3.10.

Table 3.10: A summary of all the corrosion products formed within Chapter 3.

Sample		Appearance	Elements present (EDX)	Possible compound (XRD)
	(a)	Stainless steel surface with grain boundaries	Fe	Stainless steel bulk
1 day, 1 week, 3 week (repeat), 4 week, 6 week.	(b)	Thick and flat layer	Chromium and oxygen	$LiCrO_2$
	(c)	Textured surface		Stainless steel bulk
3 week (repeat), 6 week	(d)	Large, thick layer	Iron and oxygen	Iron oxide
3 week	(e)	Blocky product	Chromium and oxygen	Fe_3O_4, FeO, Cr_2O_3, $Cr_{0.75}Fe_{1.25}O_3$. Possibly $KCrO_2$ and $FeCl_2$
	(f)	Flat corrosion product	Iron, chromium, oxygen and chlorine (similar to g, little contrast). Point analysis suggests that iron is preferentially leached	
	(g)	Initially believed to be the bulk.	Iron and chlorine	
	(h)	Flat corrosion product, but thicker and more textured than (f) and (g).	Iron and oxygen	
	(i)	Intermixing of (e) and (f). Small crystals embedded on a flat surface.	Chromium and oxygen.	

3.3: Conclusions

This chapter aimed to address how stainless steel corroded in the presence of a ternary molten chloride salt. Two different experiments were run; a baseline and a longer-duration run, both with stainless steel 316L in a ternary eutectic salt. The baseline test showed the formation of a thick lithium chromium oxide layer on the surface. The EDX data as analysed by the instrument software suggested that manganese was present in the thick corrosion layer, but further analysis concluded that this peak was caused by an overlap of the K_α peak for manganese with the K_β peak for chromium, and so chromium was the key element identified from both peaks.

The stainless steel 316L tests showed consistent results, if the three week tests are omitted, with the formation of a lithium chromium oxide layer. The EDX data for the three (repeat) and six week samples showed the formation of iron oxide on the surface and the cross section SEM for the six week test showed the iron oxide diffusing into the bulk.

The samples from the three week tests were brittle and showed the formation of numerous oxides, and due to the textured surface of the sample EDX analysis was difficult. The XRD pattern showed a distinct lack of the lithium-containing product peak at 18° 2θ, implying that lithium is essential for a stable protective layer.

It is clear that under the correct conditions it is possible for stainless steel 316L to withstand the extreme environment presented in a molten chloride environment. Chromium aids in the formation of the protective layer on the surface. Each of the samples (excluding the anomalous result obtained at three weeks) has formed a corrosion layer containing lithium, therefore it has been decided that investigating the effect of lithium on the formation of a corrosion layer in this environment would be advantageous. Chapter 4 will investigate stainless steel 316L in a ternary salt containing lithium and a binary salt where it is omitted.

Literature cited
1. L.S. Richardson, D.C. Vreeland, and W.D. Manly, *Corrosion of Molten Fluorides.* Oak Ridge National Laboratory, 1952. **ORNL-1491**.
2. A.R. Shankar and U.K. Mudali, *Corrosion of type 316L stainless steel in molten LiCl–KCl salt.* Materials and Corrosion, 2008. **59**(11): p. 878-882.
3. R.S. Sellers, M.H. Anderson, K. Sridharan, and T.R. Allen, *Failure analysis of 316L stainless steel crucible by molten fluoride salt interaction with clay bonded silicon carbide.* Engineering Failure Analysis, 2014. **42**: p. 38-44.
4. A. Nishikata, H. Numata, and T. Tsuru, *Electrochemistry of molten salt corrosion.* Materials Science and Engineering: A, 1991. **146**(1): p. 15-31.
5. K. Sridharan and T.R. Allen, *Corrosion in Molten Salts* in *Molten Salts Chemistry*, H. Groult and F. Lantelme, Editors. 2013, Elsevier: Oxford. p. 241-267.
6. L. Olson, K. Sridharan, M. Anderson, and T. Allen, *Intergranular corrosion of high temperature alloys in molten fluoride salts.* Materials at High Temperatures, 2010. **27**(2): p. 145-149.
7. C.J. Rao, A.R. Shankar, P.K. Ajikumar, M. Kamruddin, C. Mallika, and U.K. Mudali, *Corrosion Behavior of Structural Materials in LiCl-KCl Molten Salt by Thermogravimetric Study.* Corrosion, 2015. **71**(4): p. 502-509.
8. F. Subari, H.F. Maksom, and A. Zawawi, *Corrosion Behavior of Eutectic Molten Salt solution on Stainless Steel 316L.* Procedia - Social and Behavioral Sciences, 2015. **195**: p. 2699-2708.
9. A. Thompson, D. Vaughan, J. Kirz, D. Attwood, E. Gullikson, M. Howells, K.-J. Kim, J. Kortright, I. Lindau, P. Pianetta, A. Robinson, J. Underwood, G. Williams, and H. Winick, *X-Ray Data Booklet*. Centre for X-ray optics and advanced light source. 2001, Lawrence Berkeley National Laboratory.
10. J.H. DeVan, *Effect of Alloying Addtions on Corrosion Behavior of Nickel-Molybdenum Alloys in Fused Fluoride Mixtures (thesis)*. 1969, Oak Ridge National Laboratory
11. A.M. Kruizenga, *Corrosion Mechanisms in Chloride and Carbonate Salts*. 2012, Sandia National Laboratories.

12.   J.R. Reiser, J.H. DeVan, and E.J. Lawrence, *Compatibility of molten salts with type 316 stainless steel and lithium.* Journal of Nuclear Materials, 1979. **85**: p. 295-298.

13.   J. William D. Callister and D.G. Rethwisch, *Materials Science and Engineering. An Introduction*. Seventh ed. 2007: John Wiley & Sons.

14.   J.R. Davis, *Stainless Steels*. ASM Specialty Handbook (R) 1999: ASM International.

15.   N. Hiramatsu, Y. Uematsu, T. Tanaka, and M. Kinugasa, *Effects of alloying elements on NaCl-induced hot corrosion of stainless steels.* Proceedings of the 2nd International symposium on High Temperature Corrosion of Advanced Materials and Coatings, Materials Science and Engineering: A, 1989. **120**: p. 319-328.

16.   Y. Shinata, F. Takahashi, and K. Hashiura, *Proceedings of the First International Symposium on High Temperature Corrosion of Materials and Coatings for Energy Systems and Turboengines NaCl-induced hot corrosion of stainless steels.* Materials Science and Engineering, 1987. **87**: p. 399-405.

17.   A. Kruizenga and D. Gill, *Corrosion of Iron Stainless Steels in Molten Nitrate Salt.* Energy Procedia, 2014. **49**(0): p. 878-887.

18.   W.-J. Cheng, D.-J. Chen, and C.-J. Wang, *High-temperature corrosion of Cr–Mo steel in molten $LiNO_3$–$NaNO_3$–KNO_3 eutectic salt for thermal energy storage.* Solar Energy Materials and Solar Cells, 2015. **132**: p. 563-569.

19.   P. Biedenkopf, M. Spiegel, and H.J. Grabke, *High temperature corrosion of low and high alloy steels under molten carbonate fuel cell conditions.* Materials and Corrosion, 1997. **48**(8): p. 477-488.